# TTF FEL beam-based alignment by dispersion correction using Micado algorithm

P. Castro

August 19, 1997

**Abstract**

A possible method to obtain the required beam alignment in the TTF FEL undulator is to correct the dispersion using a Micado algorithm. Computer simulations including quadrupole misalignment, dipole field errors and beam position monitor errors have been used to predict the beam trajectory rms, angle rms and the required corrector current. The possibility of reducing the number of correctors and beam position monitors is investigated. Beam alignment results versus beam energy, $\Delta E/E$ of dispersion measurements, monitor resolution, shimming length, position of monitors, length of correctors and module misalignment are presented.

## 1 Introduction

The Free Electron Laser (FEL) of the TESLA Test Facility (TTF) [1] is designed to produce radiation in the spectral range of the VUV and soft X-rays. The power and the coherency of the radiation can be enhanced in the interaction between the bunch of electrons and the photons emitted at the first part of the undulator. This process is known as Self Amplified Spontaneous Emission (SASE) [2]. The amplification starts at some position in the entrance part of the undulator and reaches a saturation value for a given undulator structure.

Small transverse and longitudinal beam emittances are essential to reach saturation within a reasonable undulator length. In order to achieve the beam sizes required, quadrupoles made of permanent magnets are installed in the undulator. However, quadrupole misalignment creates orbit distortions which deteriorate the beam alignment inside the undulator and therefore the overlap of photons with the bunch of electrons. In order to correct these distortions, the FEL undulator will be equipped with beam position monitors and correctors. The tolerance limit on the beam orbit rms (with respect to a straight reference line) is around 10 $\mu$m [3]. Larger orbit rms values limit the power gain of the undulator.

A dispersion correction scheme proposed by R. Brinkmann using the Micado algorithm has been investigated for the FEL beam alignment problem. In this study we have initially considered having one monitor and one corrector (for both planes) per quadrupole. Orbit correction simulations including quadrupole misalignment, dipole field errors and beam position monitor resolution have been carried out for a diverse set of parameters as energy shift for "dispersion measurements", number of period lengths for undulator field correction (shimming), monitor resolution, number of monitors and correctors.

# 2 Basic principle of dispersion correction

The alignment of the beam with respect to a given physical reference line is feasible provided we have a beam position monitoring system with enough resolution. However, it is very difficult to obtain an absolute reference system aligned with the precision required at the FEL. Mechanical and electronic offsets of beam position monitors are in the order of 0.1 mm. Beam-based alignment methods which measure these offsets with respect to quadrupoles by changing quadrupole strengths [4] can not be applied since the quadrupoles used in the TTF-FEL are made of permanent magnetic material.

Following an idea of K. Floettmann and B. Faatz, the beam trajectory can be moved onto a straight line by steering the orbit until the dispersion vanishes, provided that dispersion and its derivative are zero at the entrance of the FEL. Since the dispersion is obtained as the orbit difference between beams with different energy, this method is independent of beam position monitor offsets. The differential equation of the dispersion function has an expression similar to the differential equation of the beam trajectory and dispersion errors propagates like orbit errors. Therefore, the same algorithms used for orbit correction can be envisaged for dispersion correction.

The problem to find a set of corrector strengths which corrects to zero the beam position (or the dispersion) observed at the beam position monitors can be expressed as the following system of linear equations

$$d_i + \sum_{j=1}^{N_{\text{corr}}} a_{ij} c_j = 0 \qquad \text{for } i = 1, ..., N_{\text{mon}} \tag{1}$$

where $N_{\text{mon}}$ and $N_{\text{corr}}$ are the number of monitors and correctors (in the FEL $N_{\text{mon}} = N_{\text{corr}}$). The unknown $c_j$ is the corrector strength and $d_i$ is the measured beam position (in our case dispersion) at the monitors. The *corrector matrix* coefficient $a_{ij}$ is calculated as the effect of the strength of corrector $j$ on the beam orbit (dispersion) at monitor $i$.

Micado [5] is an algorithm used to correct the orbit in storage rings. This algorithm is designed for any number of monitors and correctors. Micado uses the method of "the best correctors" to search for a set of correctors strengths that minimizes the norm of residual vector defined as

$$r_i = d_i + \sum_{j=1}^{N_{\text{corr}}} a_{ij} c_j$$

A set of correctors is obtained by either specifying the maximum number of correctors to be used or giving a maximum value for the norm of the residual vector.

The *dispersion* function is defined as the energy dependence of the transverse beam position

$$D_x(s) = \frac{dx(s)}{dE/E} \qquad D'_x(s) = \frac{dx'(s)}{dE/E}$$

where $D'_x(s)$ is the dispersion derivative which represents the energy dependence of the transverse angle of the beam trajectory. Without dipole field errors and with a perfect quadrupole alignment in the FEL, the dispersion function is given by the undulator magnetic structure. The dipoles of the undulator create dispersion that vanishes every period length. Dipole field errors or quadrupole misalignment introduce dispersion which propagates downstream like orbit errors.

In order to simulate dispersion measurements including a finite monitor resolution, a $\Delta E/E$ of 20% is taken. Beam orbit measurements at $E$ and at $E - \Delta E$ provide a "dispersion measurement"

at the beam position monitors:

$$d_x(s_i) = \frac{x_i(E - \Delta E) - x_i(E)}{\Delta E/E} \qquad \text{for } i = 1, ..., N_{\text{mon}}$$

The orbit offset thus obtained corresponds to the values of the linear dispersion $D_x(s_i)$ plus a higher order contribution from the change of the phase due to chromaticity. The correction matrix used in the simulations is calculated by

$$a_{ij} = d_x(s_i)|_{(c_j=1)}$$

These coefficients have to be numerically calculated for the same $\Delta E$ used in the "dispersion measurement". The dispersion can not be corrected if the difference between $\Delta E/E$ for measured dispersion and for $a_{ij}$ is more than 10%.

# 3 FEL undulator

In the first phase of the FEL, an undulator of 15 m long [6] will be installed at the end of the accelerator section of the TTF. The TTF will provide a beam energy of about 390 MeV (although the first tests of the FEL are at 300 MeV). In the phase II the energy provided by the accelerator will be around 1 GeV and the undulator will be extended to 30 m [7]. The possibility of a 40 m long undulator for a beam energy of 2 GeV is also envisaged [8].

The undulator is subdivided into modules of about 4.5 m length. Each module has 327 poles (iron plates) separated by blocks of dipole magnets. The undulator creates a sinusoidal field of 0.5 T peak value with a period of $\lambda_u = 27.3$ mm. It corresponds to two dipole magnets.

The focusing structure of the FEL is provided with ten quadrupoles per module with alternating focusing gradients (starting by a horizontal focusing quadrupole). The quadrupoles are $5\lambda_u$ long and their integrated strength is 2.5 T (which corresponds to a gradient of $g = 18.3$ Tm$^{-1}$). The distance between focusing and defocusing quadrupoles is $12.5\lambda_u$. The optics parameters of this periodic lattice at 300 MeV, 390 MeV and 1 GeV (for phase II) are shown in table 1, where $k$ is the quadrupole strength and $f$ its focal length (for a thick quadrupole):

$$k = e\,c\,\frac{g}{E} \simeq 0.3\,\frac{g[\text{T/m}]}{E[\text{GeV}]} \qquad \frac{1}{f} = \sqrt{k}\,\sin\left(\sqrt{k}\,L\right)$$

where $L$ is the length of the quadrupole. The maximum and the minimum of the $\beta$ function are located at the focusing and the defocusing quadrupoles, respectively. The $\beta$ function and $\phi$ (the phase advance between the center of two focusing or two defocusing quadrupoles) are calculated using transport matrices for thick quadrupoles.

The weak focusing of the undulator of length $l$ is

$$\frac{1}{f_{\text{weak}}[\text{m}]} \simeq 0.45\,l[\text{m}]\,\frac{B_o^2[\text{T}^2]}{E^2[\text{GeV}^2]}$$

For $l = 17.5\lambda_u = 0.478$ m, we obtain $f_{\text{weak}} = 1.67$ m at 300 MeV and $f_{\text{weak}} = 18.6$ m at 1 GeV. Since these values are larger than the focusing length of the quadrupoles, the weak focusing is not included in the simulations.

In the orbit correction simulations, we have taken initially one beam position monitor and one corrector per quadrupole in the FEL. A side view of the layout of magnets and monitors inside the gap of the undulator is shown in fig. 1.

| $E$ | 300 MeV | 390 MeV | 1 GeV |
|---|---|---|---|
| $k$ [m$^{-2}$] | 18.3 | 14.1 | 5.5 |
| $f$ [m] | 0.42 | 0.54 | 1.35 |
| $\beta_{\max}$ [m] | 1.58 | 1.76 | 3.46 |
| $\beta_{\min}$ [m] | 0.50 | 0.76 | 2.54 |
| $\phi_{\mathrm{FODO}}$ | 65° | 49° | 18.5° |

Table 1: Optics parameters for the FEL lattice. For symbol description refer to the text.

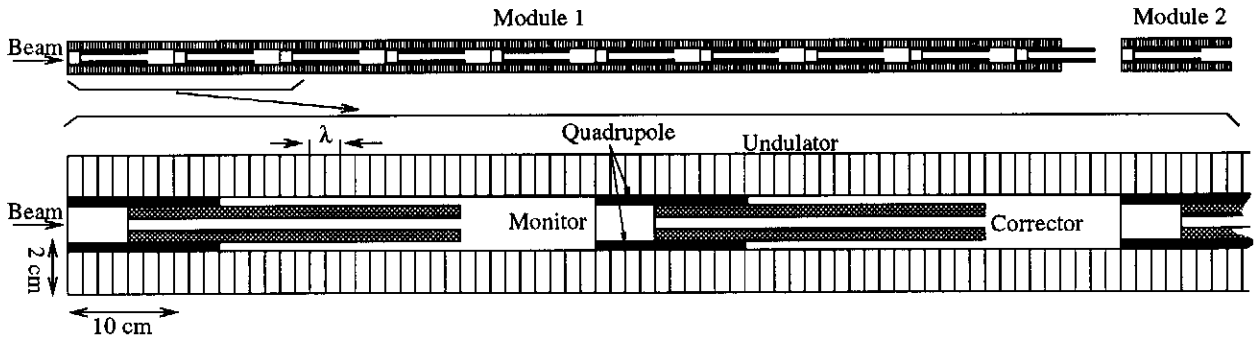


Figure 1: Side view of one of the three modules of the FEL (top picture) and of one FODO cell (bottom picture) showing the location of beam position monitors, corrector coils and quadrupoles. All dimensions of the elements are to scale approximately, except the length of the monitors of about 10 cm.

A beam position monitor block of the FEL consists of two pairs of electrodes separated by $1.5\lambda_u$. The total length of the monitor block is about 10 cm. Both horizontal and vertical orbits (and dispersion) are calculated at the center of the monitor, one $\lambda_u$ behind the entrance position of the quadrupole and two $\lambda_u$ in front of the entrance position of the corrector.

The correctors of the FEL undulator consist of four wires which can be powered independently to provide a horizontal and a vertical dipole field. The location of the wires in the undulator magnet is shown in fig. 2. The copper wires have a rectangular cross section of $4 \times 4$ mm with a 2.5 mm hole for water cooling of the wires.

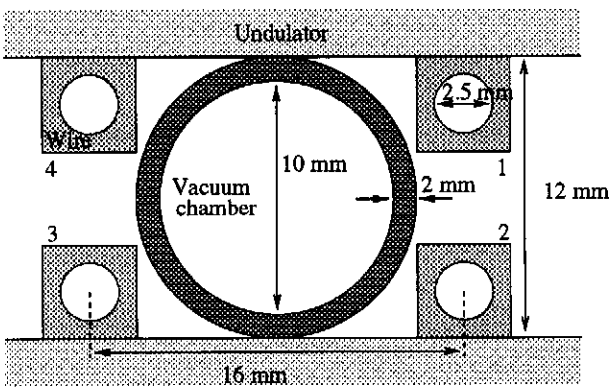


Figure 2: Cross section of the FEL undulator indicating the location of the four wires which create horizontal and vertical dipole corrector fields.

The current needed to create a horizontal field of 1 mT is $I_h = 25$ A and to create a vertical field of 1 mT is $I_v = 12.5$ A. In each case, only one power supply is needed for the four wires. The corrector can be used for both horizontal and vertical orbit correction with two power supplies:

One connected to the wires 1 and 3 (numbers being indicated in fig. 2) which have the same current $I_h - I_v$ and opposite polarity and one connected to the wires 2 and 4 which have same current $I_h + I_v$ and opposite polarity.

The bending radius of the beam trajectory is given by

$$\frac{1}{r} = c\,e\,\frac{B}{E} \simeq 0.3\,\frac{B[\mathrm{T}]}{E[\mathrm{GeV}]}$$

The corrector length assumed in the simulations is 30 cm ($11\lambda_u$), which allows (at 300 MeV) a steering power of 24 and 12 $\mu$rad/A in the horizontal and vertical planes respectively.

# 4 Implementation of errors in the simulation

**Quadrupole misalignment** Quadrupoles are made of permanent magnets that can be aligned better than $\pm 50$ $\mu$m. In the simulations, horizontal and vertical quadrupole offsets from a reference line are randomly generated with a flat distribution function between $-50$ and 50 $\mu$m.

**Dipole field errors** The undulator (vertical) field is supposed to vary along the longitudinal axis as:

$$B(s) = B_o \sin\left(\frac{2\pi s}{\lambda_u}\right)$$

where the *peak field* $B_o$ is 0.5 T. The peak field error is believed to be about $\Delta B/B_o = 4 \cdot 10^{-3}$ rms or lower. Random dipole field errors in the undulator have been computed in the simulations as an equivalent horizontal orbit kick $\alpha$ at the iron plate (where the dipole field is maximum)

$$\alpha = \frac{c\,e}{E}\int_{\lambda_u/2} \Delta B(s)\,ds$$

For $\Delta B = 2$ mT the orbit deflection over half period length is $\alpha = 17.4$ $\mu$rad.

Amplitude field errors of dipoles only affect the horizontal trajectory of the beam. Tilt errors on the alignment of the iron poles introduce horizontal field errors that affect the vertical trajectory. A $\Delta B_h = 2$ mT rms is included in the simulations.

The technique used in the fabrication process of the undulator known as shimming of dipole field errors has been applied to the set of random orbit kicks generated in the simulations. This technique consists of measuring the integrated field of the undulator and compensating for the effect of orbit deflection and orbit displacement due to dipole field errors. In this process, the integrals

$$\int_o^{n\lambda_u} B(s)\,ds \qquad \text{and} \qquad \int_o^{n\lambda_u}\left(\int_o^s B(z)\,dz\right)ds$$

are evaluated over a certain number $n$ of period lengths of the undulator. The first field integral measures the total orbit deflection of $n$ period lengths. The second field integral represents the orbit displacement. In the simulations, the equivalent integrals are calculated by

$$S_1 = \sum_{i=1}^{2n} \alpha_i \qquad \text{and} \qquad S_2 = \sum_{i=1}^{2n} \alpha_i (2n-i)\lambda_u/2$$

where $\alpha_i$ is the random orbit kick at dipole $i$. The sums $S_2$ and $S_1$ are compensated by adding orbit kicks at the first and the last dipoles, respectively:

$$\Delta\alpha_1 = \frac{-S_2}{(2n-1)\lambda_u/2} \qquad \text{and} \qquad \Delta\alpha_{2n} = -S_1 - \Delta\alpha_1$$

Both $S_2$ and $S_1$ are corrected to exactly zero in the simulations. Note that in the case $n$ is set to one, i.e. $S_2$ and $S_1$ are compensated for every period length, all kick errors are corrected.

**Monitor resolution** Monitor offsets (systematic errors in beam position measurements) are not taken into account since only difference orbits are calculated. Only statistical errors on the beam position measurement are included as 1 $\mu$m rms (1.4 $\mu$m rms for the difference orbit). Scaling errors (electronic calibration errors) are not included, since their effect on the correction becomes small after some iterations.

# 5 An example of dispersion correction

In order to illustrate the orbit alignment by dispersion correction using Micado, an example is taken for a simulation including quadrupole misalignment of $|\Delta x, y| \leq 50$ $\mu$m, dipole field errors of $\Delta B = 2$ mT rms (0.4% of $B_o$) and 1 $\mu$m rms monitor resolution. Dipole field integrals are corrected every $10\lambda_u$. The position and the angle of the beam as well as $D(s)$ and $D'(s)$ are zero at the entrance of the first FEL module. The beam energy is 390 MeV and an energy of 312 MeV ($-20\%$) is taken to "measure" the dispersion at the monitors.

The horizontal orbit and the horizontal dispersion of the uncorrected and corrected systems are shown in fig. 3. The horizontal orbit rms of the uncorrected system is 0.22 mm and the dispersion rms is 1.43 mm. After correction, the dispersion rms is 8.4 $\mu$m and the orbit rms is 16.9 $\mu$m (15.7 $\mu$m rms if fitted to a straight line).

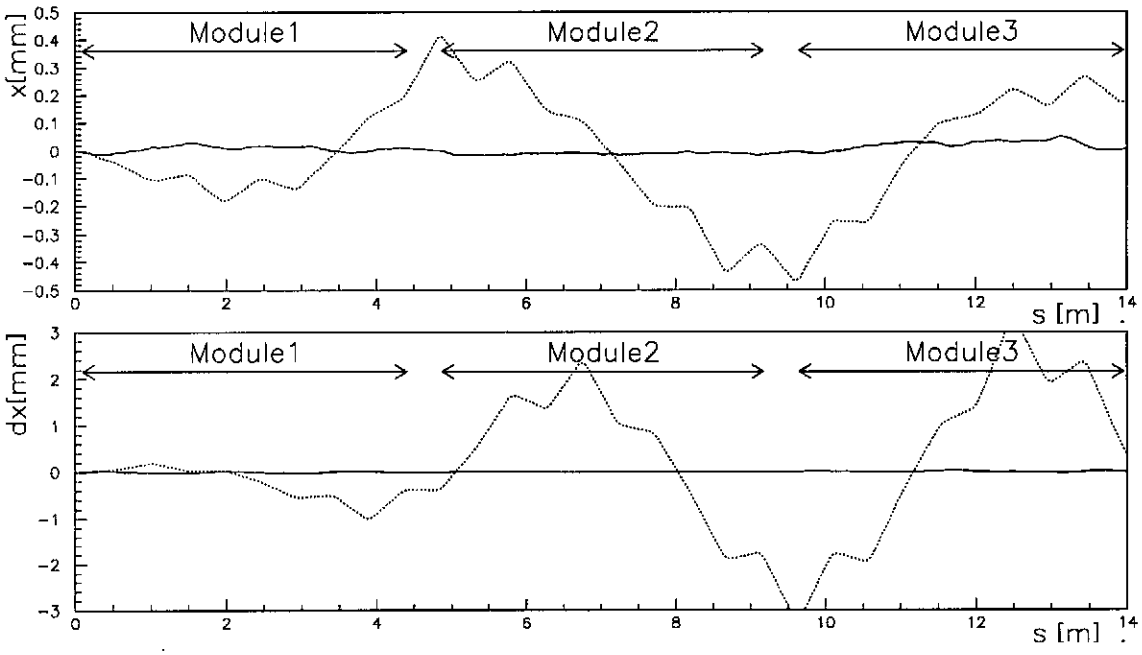


Figure 3: Orbit $x$ (top plot) and dispersion $d_x$ calculated for $\Delta E/E = 20\%$ (bottom plot) through the three FEL modules before (dashed line) and after correction (full line).

The correction, using 30 H/V correctors and 30 monitors, was stopped after 15 iterations with Micado algorithm, using for each correction iteration five correctors. Corrections with more than five correctors per iteration lead to large orbit distortions. The horizontal orbit rms (the mean value over 1000 random seeds) as a function of the number of iterations with Micado is shown in fig. 4. Each line corresponds to simulations for which 5, 8, 10 and 15 correctors per

iteration have been taken. Although corrections with more than five correctors provide corrected orbits with low rms results at the first iterations, further iterations systematically increase the orbit rms and create large orbit distortions. This effect is discussed in section 8.

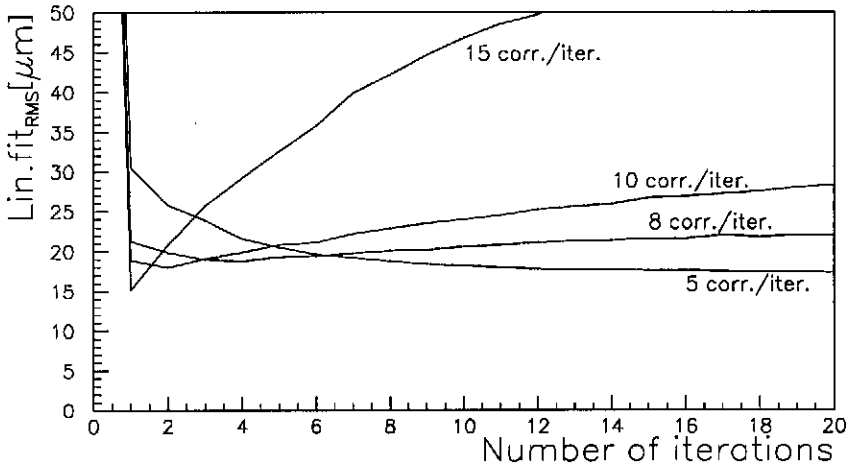


Figure 4: Linear fit rms (mean over 1000 seeds) of the horizontal orbit as a function of the number of correction iterations applied with 5, 8, 10 and 15 correctors per iteration.

# 6 How many correctors are needed?

Based on simulation results, the efficiency of the dispersion correction scheme using Micado algorithm is improved when only the correctors located at focusing quadrupoles are used. The effects observed with one corrector every two quadrupoles are the following:

1. The corrected orbit rms is about 30% smaller than in simulations with one corrector per quadrupole.

2. The average rms of corrector strengths is a factor two smaller than in simulations with one corrector per quadrupole.

3. A set of corrector strengths which minimizes the dispersion rms (and the orbit rms) is obtained with one correction iteration with all 15 correctors. Further iterations do not increase nor reduce the corrected orbit rms, it only varies due to monitor statistical errors. A detailed discussion on the effect of dispersion correction with fewer correctors is given in section 8.

**Corrector configuration**

The orbit rms obtained in simulations with correctors at focusing quadrupoles is smaller than with correctors in all quadrupoles. Simulation results on corrected horizontal and vertical orbit rms (averaged over 1000 seeds) are shown in table 2 for three corrector configurations.

The results presented in table 2 correspond to simulations with the following correctors:

- 30H/30V configuration, with horizontal and vertical correctors every quadrupole.

- 15H/14V configuration, with horizontal correctors only at horizontal focusing quadrupoles (odd numbers) and with vertical correctors only at vertical focusing quadrupoles (even numbers). Only 14 vertical correctors are actually used because the corrector at the last quadrupole (number 30) is disabled (since there is no monitor downstream).

| Num. corr. | Location | $x_{\rm rms}$ [$\mu$m] | $y_{\rm rms}$ [$\mu$m] |
|---|---|---|---|
| 30H/30V | QF and QD | 17.3(15.3) | 18.2(14.8) |
| 15H/14V | QF | 11.6(9.7) | 11.7(11.0) |
| 16H/15V | QF+1st QD | 11.7(9.8) | 10.5(9.7) |

Table 2: Average of the orbit position $x, y$ rms (linear fit) as a function of the number of correctors. These results were obtained from simulations with 30 monitors. Values in parenthesis are results from simulations with 31 monitors (one monitor added at the end of the FEL). Refer to the text for corrector configuration.

- 16H/15V configuration, with one more corrector per plane than in the 15H/14V configuration: both first and second correctors are used in horizontal and vertical corrections. The layout of correctors is shown schematically in fig. 5.

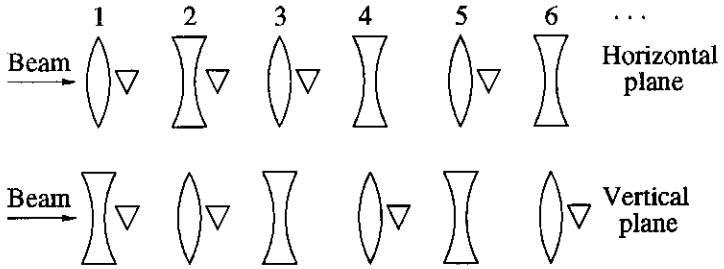


Figure 5: Sketch of the corrector configuration 16H/15V with the first two correctors for horizontal and vertical planes. Triangles represent correctors.

With the 15H/14V and 16H/15V configurations the number of correctors is the same as with 30H/30V, but the number of power supplies employed is reduced by half.

At 390 MeV the results obtained with 16H/15V configuration in the vertical plane are better than with 15H/14V. On the horizontal plane the results are similar with 15H/14V and 16H/15V configurations. However, at beam energies about 1.4 GeV the results with 16H/15V configuration are better. The corrected horizontal and vertical orbit rms are shown in fig. 6 as function of beam energy for simulations with the three corrector configurations.

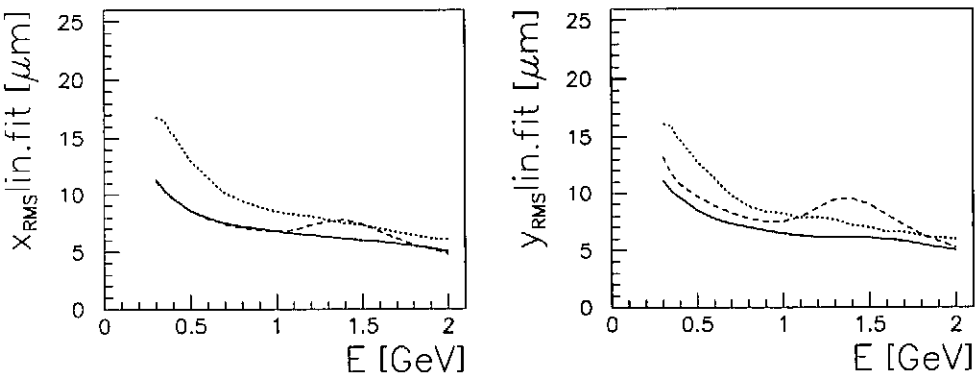


Figure 6: Mean orbit $x, y$ rms (linear fit) for 1000 simulations as function of the beam energy for three corrector configurations: 30H/30V (dotted line), 15H/14V (dashed line) and 16H/15V (solid line).

As expected, the effect of dipole errors and quadrupole misalignment on the beam orbit is smaller for higher energies. However, simulation results with 15H/14V configuration present

a relative increase of the horizontal and vertical rms between 1.0 and 1.4 GeV. Although no satisfactory explanation has been found, this resonance appears to be related to the phase advance of 180° over the three modules of the FEL for the energy $E - \Delta E$, i.e. the energy for "dispersion measurements".

### Corrector current

The rms current per corrector (over 10000 seeds) in simulations with 30H/30V and 16H/15V configurations are shown in fig. 7.

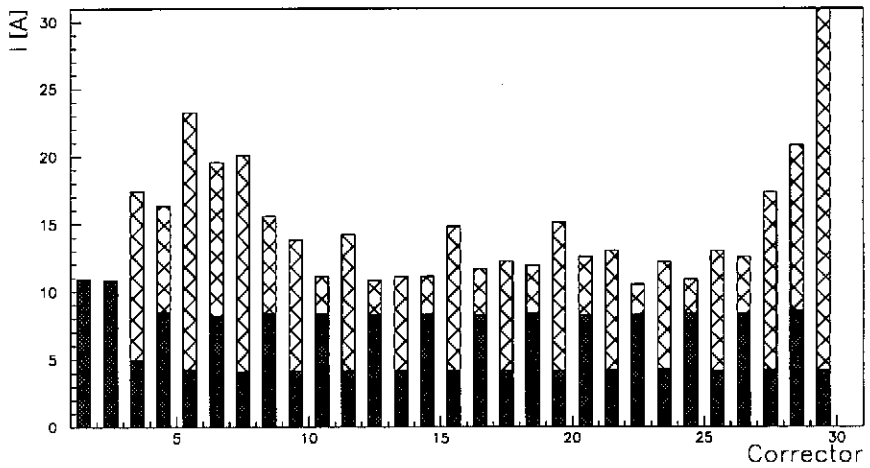


Figure 7: Rms current per corrector in 1000 simulations with 30H/30V (crossed area) and with 16H/15V correctors (solid area).

Except for the first two correctors, which are horizontal and vertical, the bending field rms is the same for all correctors. The current rms is about 4.2 A for horizontal correctors and 8.3 A for vertical correctors. The current rms for the first two correctors is about 10.8 A.

In order to specify the maximum current required for the power supplies of the FEL, the distribution of corrector currents for 10000 seeds is shown in fig. 8.

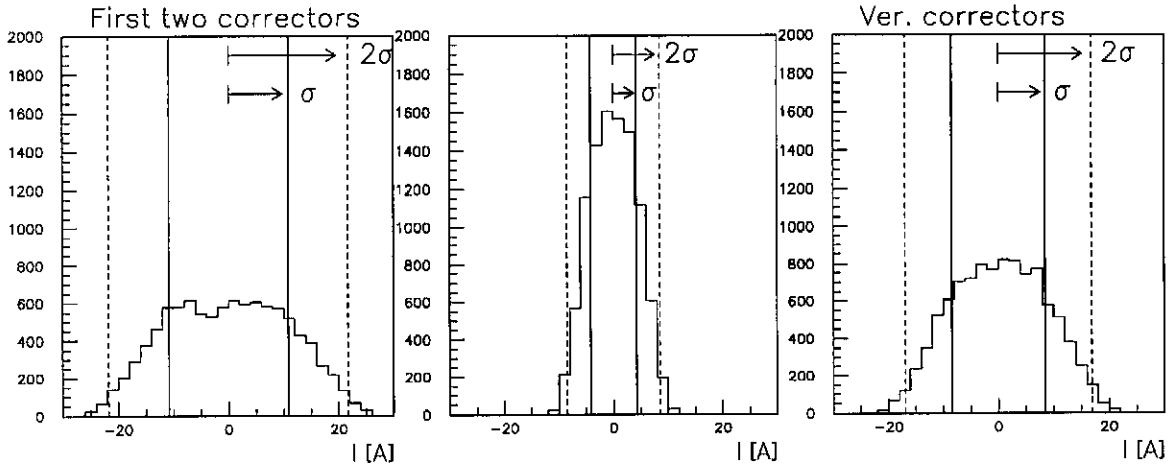


Figure 8: Current distribution of the first corrector (left), for vertical correctors (middle) and for horizontal correctors (right) in the orbit correction simulations for 10000 seeds using 16H/15V correctors. Vertical lines indicate $\pm\sigma$ (solid lines) and $\pm 2\sigma$ (dashed lines) for $\sigma$ = 10.8, 4.2 and 8.3 A, respectively.

# 7 How many monitors are needed?

The results shown in table 2 are from simulations using the 30 monitors of the FEL. The results between parenthesis are obtained from simulations including one monitor at the end of the FEL as it was found that the corrected orbit rms is in average 15% lower. The orbit rms obtained with 31 monitors as a function of the beam energy is compared in fig. 9 with results obtained with 30, 32 and 33 monitors. Simulations including a second and a third monitor at the end of the FEL show no significant improvements in the corrected orbit.

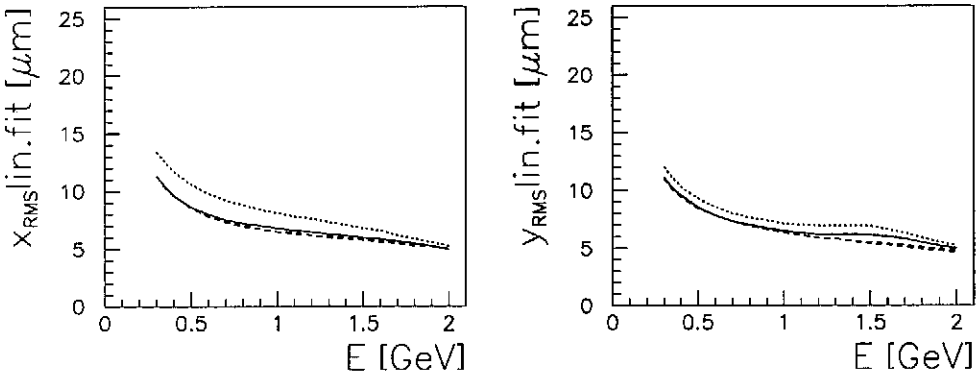


Figure 9: Mean orbit rms (linear fit) as function of the beam energy for simulations with 30 (dotted line), 31 (solid line), 32 and 33 monitors (dashed lines).

With the corrector configuration 16H/15V, it is possible to reduce the number of monitors in the simulations from 31 to 16 without decreasing the performance of the correction. Simulation results with 31, 18, 17 and 16 monitors are listed in table 3.

| $N_{\text{mon}}$ | Config. | List of monitors | $x_{\text{rms}}$ [$\mu$m] | $y_{\text{rms}}$ [$\mu$m] |
|---|---|---|---|---|
| 31 | 31 mon. | 1,2,3,...,29,30,31 | 9.8 | 9.7 |
| 18 | 18HQF | 3,5,7,9,...,25,26,27,28,29,30,31 | 9.9 | 10.9 |
| 17 | 17HQF | 3,5,7,9,...,25, 27,28,29,30,31 | 9.9 | 11.1 |
| 16 | 16HQF | 3,5,7,9,...,25, 27, 29,30,31 | 10.1 | 11.1 |
| 18 | 18VQF | 2,4,6,8,...,26,27,28,29,30,31 | 11.1 | 9.8 |
| 17 | 17VQF | 2,4,6,8,...,26, 28,29,30,31 | 11.3 | 9.8 |
| 16 | 16VQF | 2,4,6,8,...,26, 28, 30,31 | 48* | 9.9 |

Table 3: Average of the orbit position $x, y$ rms (linear fit) as a function of the number of monitors (for $E = 390$ MeV and $\Delta E/E = 20\%$). (*) This value is obtained after 20 iterations using Micado with three correctors per iteration.

Since it is not possible to dissociate the horizontal and the vertical measurements of the beam position monitors, the only possibility to reduce the number of monitors is to place them either at the horizontal focusing quadrupoles (even numbers) or at the vertical focusing quadrupoles (odd numbers). In simulations at 390 MeV, if only the monitors placed at horizontal focusing quadrupoles are used (configuration 16HQF), the horizontal orbit rms increases up to 3%. In the vertical plane, the orbit rms increases up to 14%. The monitor configuration 16HQF is shown schematically in fig. 10.

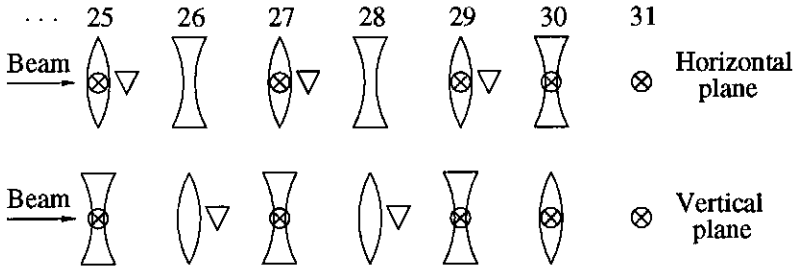


Figure 10: Sketch of the corrector configuration 16H/15V and monitor configuration 16HQF at the end of the FEL. Triangles represent correctors and crossed circles represent monitors.

If only the monitors placed at vertical focusing quadrupoles are used (configuration 17VQF), the vertical orbit rms increases up to 2% and the horizontal orbit rms becomes 15% larger. The orbit rms versus the beam energy is shown in fig. 11 for monitor configurations 16HQF, 17VQF and with 31 monitors. For higher beam energies, the difference of orbit rms becomes larger between simulations with 16HQF and 17VQF configurations and simulations with 31 monitors. The difference of corrector current rms becomes larger as well.

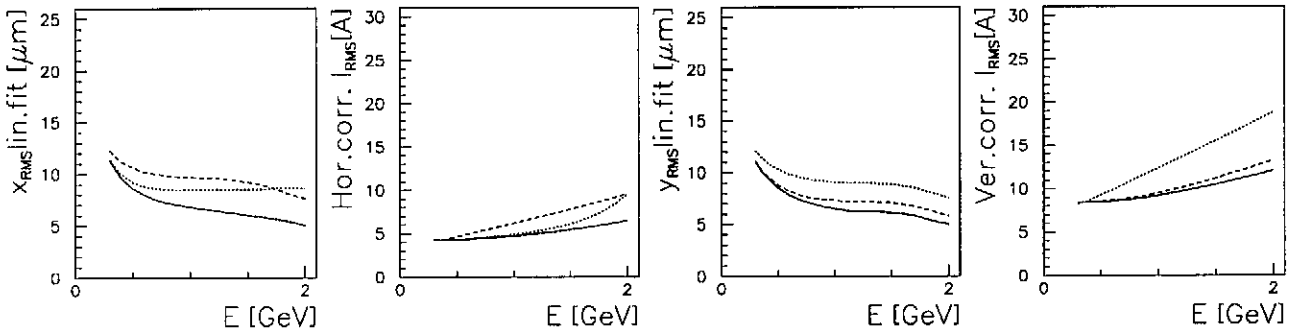


Figure 11: Mean orbit rms (linear fit) and current rms for horizontal and vertical correctors as function of the beam energy for three monitor configurations: 16HQF (dashed line), 17VQF (dotted line) and 31 monitors (solid line).

It has been also observed that:

- The corrected orbit rms does not change if the first four monitors are removed. One reason is that orbit distortions due to errors in the first module are observed as well at the monitors located in the second and in the third modules and therefore they can be corrected.
- The last two or three monitors of the FEL are needed for an effective dispersion correction.

These effects are particular for the simulation used here. The measurements provided by the first monitors are less relevant because a perfect aligned beam at the entrance of the FEL is assumed in the simulation. In a more realistic case with beam orbit errors upstream of the FEL, these first monitors are needed.

The last monitors of the FEL play a vital role for the global correction of the dispersion. At least two monitors downstream the last corrector are needed for an effective dispersion correction. As already shown in table 2, one additional monitor at the end of the FEL improves the orbit alignment. In the TTF, a line of diagnostic devices is installed behind the undulator. These monitors can be used for dispersion correction in the FEL.

# 8 Orbit and dispersion correction

We have observed in FEL beam alignment simulations that large orbit distortions are introduced sometimes (depending on the corrector and monitor configuration) by correcting the dispersion with all correctors in one iteration. In order to illustrate this situation the example of section 5 is taken. The dispersion of the uncorrected and corrected system using 30 monitors and 30 correctors per plane is shown in fig. 12. Note that the dispersion scale (vertical axis of bottom plot) is between $\pm 0.3$ mm, which is smaller than the scale used in fig. 3.

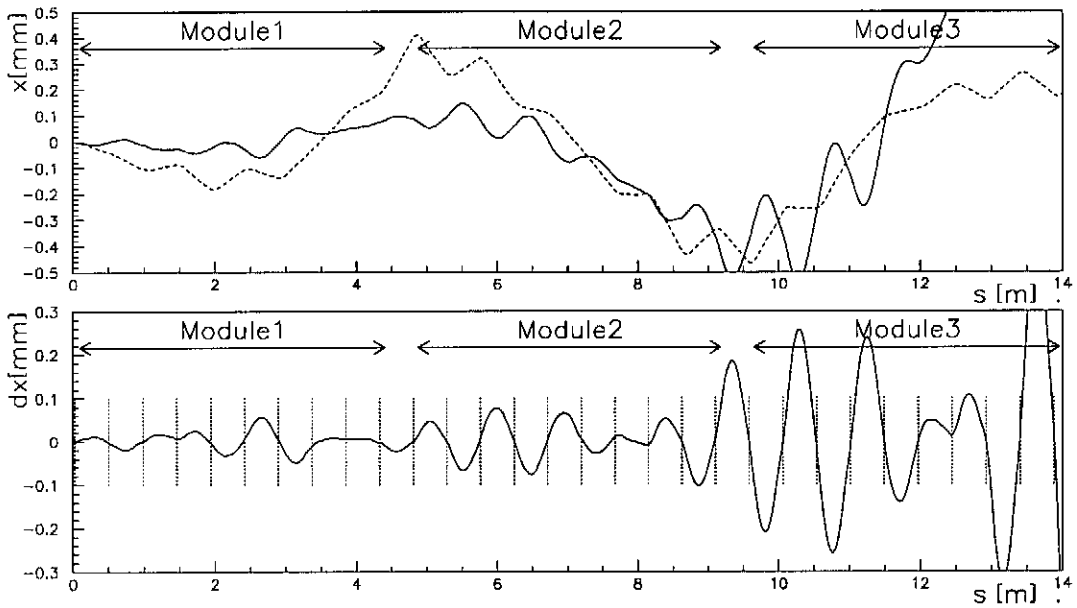


Figure 12: Orbit $x$ (top plot) and dispersion $d_x$ (bottom plot) before (dashed line) and after correction (full line) with 30 monitors and 30 correctors per iteration. Monitors location are indicated with vertical dotted lines.

The dispersion of the corrected system is 105 $\mu$m rms, while at the monitors is 6.3 $\mu$m rms. The latter corresponds (for a $\Delta E/E$=0.2) to the measurement error of beam position differences, i.e. 1.4 $\mu$m rms. That means the dispersion function is well corrected at the monitors, which are indicated with vertical dotted lines in fig. 12. However, the dispersion correction introduces dispersion bumps between monitors and leads to orbit distortions. The average amplitude of these dispersion bumps and the orbit rms depend strongly on the position of the monitors with respect to the quadrupoles and on the phase advance between monitors. Another effect is that the amplitude of the dispersion bumps grows towards the end of the FEL and therefore the orbit rms diverges. This is explained in the following way: Solving the system of linear equations for the FEL we get

$$
\begin{aligned}
d_2 + a_{21}c_1 = 0 \quad &\text{then} \quad c_1 = \frac{-d_2}{a_{21}} \\
d_3 + a_{31}c_1 + a_{32}c_2 = 0 \quad &\text{then} \quad c_2 = \frac{-d_3 - a_{31}c_1}{a_{32}} \\
&\cdots \\
d_{i+1} + \sum_{j=1}^{i} a_{i+1,j}\, c_j = 0 \quad &\text{then} \quad c_i = \frac{1}{a_{i+1,i}} \left( -d_{i+1} - \sum_{j=1}^{i-1} a_{i+1,j}\, c_j \right)
\end{aligned}
$$

The correction is made using one corrector for one monitor and the equations (on the left-hand

side) have exact solution (on the right-hand side). The first corrector cancels the dispersion measured at the second monitor. The second corrector cancels the dispersion measured at the third monitor and compensates the dispersion created by the first corrector in the third monitor, and so on. In this local dispersion correction scheme, each corrector downstream cancels then the dispersion measured at the first monitor downstream and compensates the dispersion created by the upstream correctors at this monitor. However, the dispersion derivative can have any value and the dispersion between two monitors is the sum of the dispersion created by all upstream correctors, which do not cancel. This uncorrected dispersion introduces large orbit distortions.

The correctors current in this example is shown in fig. 13. Note the vertical scale is up to 350 A. The currents increase rapidly toward the end of the undulator. The strength of the last correctors is about one order of magnitude higher than the one of the firsts correctors.

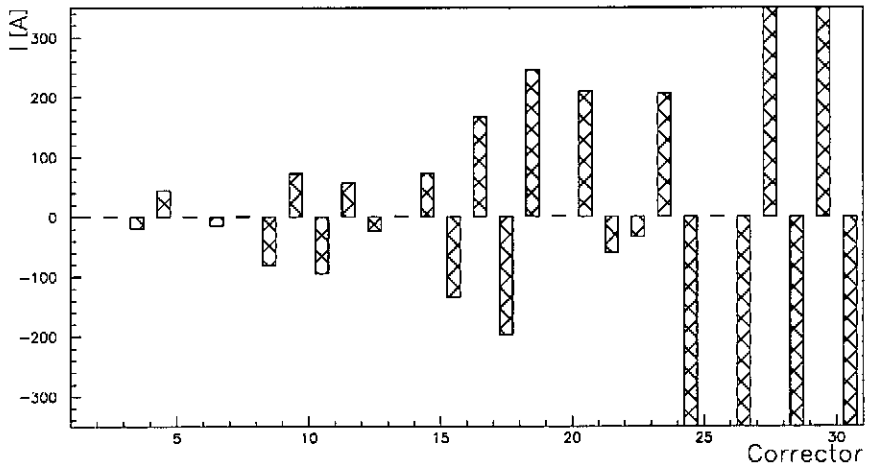


Figure 13: Current per corrector in the simulation using 30 correctors per iteration.

Dispersion bumps between monitors are avoided by limiting the number of correctors used per correction iteration to four or five. In each iteration, Micado selects a set of five corrector strengths which minimize the "global" dispersion rms at the monitors. The corrected dispersion rms obtained is in the same order as the dispersion rms at the monitors. For instance, the dispersion shown in fig. 3 is corrected to 10.5 $\mu$m rms and the dispersion at the monitors is 12.8 $\mu$m rms. Using a larger number of correctors per iteration, it is more probable to correct dispersion locally and to introduce a dispersion bump between two correctors. However, this procedure is lengthy because small orbit rms values are obtained after 15 or 20 iterations.

### Fewer correctors than monitors

Using only one corrector every two quadrupoles, the dispersion is minimized in one iteration with all correctors. Dispersion corrections with all 15 correctors per iteration do not introduce dispersion bumps and further iterations do not change in average the corrected orbit rms. The reason that this corrector configuration does not introduce dispersion bumps is the following: The first corrector is used to minimize the dispersion measured at the first two monitors downstream. The second corrector has to minimize the dispersion measured at the next two monitors and the dispersion created by the first corrector. Each corrector minimizes the dispersion measured at the next two monitors and minimizes the dispersion created by all upstream correctors. But now the correctors can not cancel the dispersion created by correctors located upstream (as it was the case with 30 correctors). Therefore, the dispersion created by correctors tends to increase the dispersion rms at all monitors downstream. Since each corrector would increase the global

dispersion rms, its strength is now calculated in order to minimize globally the dispersion at all downstream monitors. The derivative of dispersion is also minimized because the dispersion is measured by all downstream monitors, which have different phase advance with respect to each corrector.

The fact that the correction is made with one corrector for two monitors is not so relevant for a global dispersion correction. The dispersion is also minimized in one iteration with one monitor every two quadrupoles for the monitor configuration 16HQF. The dispersion correction is global because the last three monitors are used. In the monitor configuration 16HQF (see fig. 9), the monitors 29, 30 and 31 are used and the last corrector can not completely correct the dispersion at these monitors. Then, the strengths of all correctors are selected in order to minimize also the dispersion rms at the last monitors and the dispersion correction becomes global. For instance, the correction of the horizontal dispersion for the monitor configuration 16VQF, where the monitor 29 is not used (see table 3), creates dispersion bumps unless a second additional monitor at the end of the FEL is used. In this case the orbit rms obtained is 29 $\mu$m.

# 9 Simulation results

SASE process originates from the interaction between photons and electrons over a certain length in an undulator magnetic field. Therefore, the trajectory of the electron beam must be aligned onto a straight line along the undulator. In order to parameterize the alignment of the beam along the FEL, we show the results of the linear fit rms of the beam trajectory and the angle rms. The results shown in the following are the average values of these parameters over 1000 simulations.

The corrector configuration used in the simulations is 16H/15V: One corrector every focusing quadrupole. The two first correctors are both horizontal and vertical, the third is horizontal, the forth vertical and so on. The last vertical corrector (number 30) is not used. The monitors, which measure both horizontal and vertical beam positions, are located at every quadrupole.

## 9.1 Energy dependence of beam alignment results

The results presented in this paper are from simulations with three undulator modules, i.e. for the phase I of the FEL. In the phase II the FEL consists of six (or eight) modules. Results from simulations for a beam energy between 300 MeV and 2 GeV are shown in fig. 14. The simulations results for a FEL with six and eight modules are also shown.

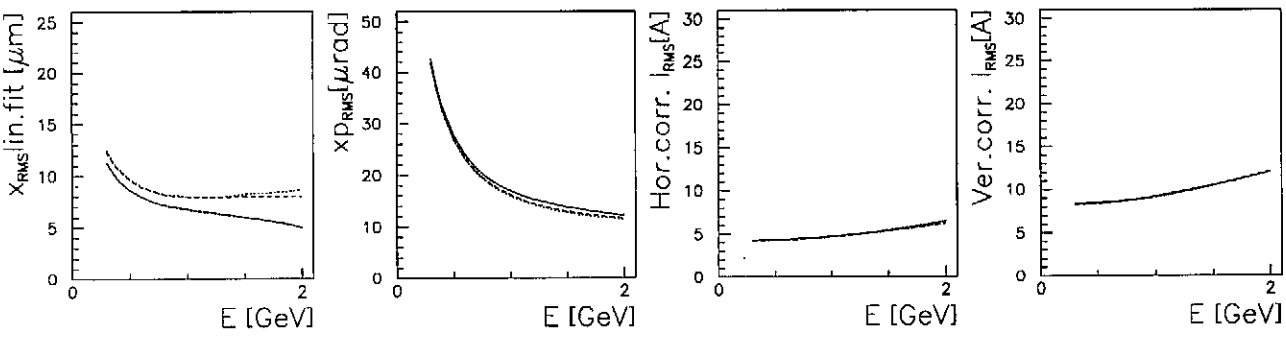


Figure 14: Mean $x_{\rm rms}$ (linear fit), $x'_{\rm rms}$ and corrector current rms as a function of the beam energy with simulations of three (solid line), six (dashed line) and eight modules (dotted line).

The results for a FEL with six and eight undulator modules are very similar. The results for a FEL with three modules are smaller because the orbit rms at the first part of the undulator is small due to the assumption of a perfect beam alignment at the entrance. Between 300 MeV and 1 GeV the orbit rms decreases as function of the beam energy as expected. At beam energies between 1 and 2 GeV, the orbit rms is practically constant.

At 1 GeV and for a FEL with six modules the horizontal orbit rms after correction is 8.0 $\mu$m. The current rms of horizontal correctors increases from 4.2 A at 300 MeV to 4.6 A at 1 GeV and to 6.2 A at 2 GeV, while the current rms of vertical correctors is a factor two higher, increasing from 8.3 A at 300 MeV to 9.1 A at 1 GeV and to 12.2 A at 2 GeV.

## 9.2 Effect of monitor resolution on beam alignment results

Beam position errors due to a finite monitor resolution affect the dispersion measurements and therefore the dispersion correction. Choosing a larger $\Delta E/E$ for dispersion measurements the effect of position measurement errors is reduced. Simulation results for a monitor resolution of 1, 2, 3, 4 and 5 $\mu$m are shown in fig. 15 as a function of $\Delta E/E$ at $E = 390$ MeV.

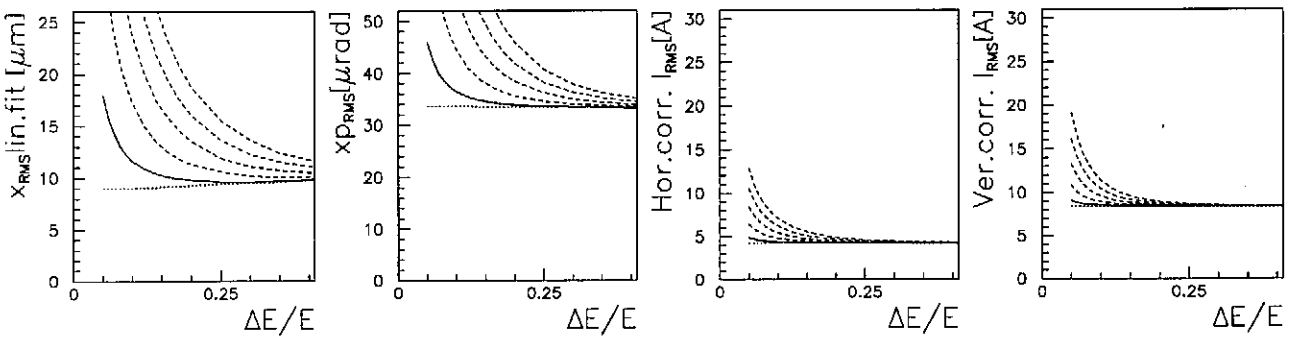


Figure 15: Mean $x_{\rm rms}$ (linear fit), $x'_{\rm rms}$ and corrector current rms as a function of $\Delta E/E$. Results for 1 $\mu$m rms monitor resolution are indicated with a solid line. The dashed lines above are the results for 2, 3, 4 and 5 $\mu$m rms. The dotted line are the results of simulations in which monitor errors are not included.

For a monitor resolution of 1 $\mu$m and a $\Delta E/E$ of 20% the effect of dispersion measurement errors on the orbit is sufficiently reduced. If position monitors have lower resolution then the corrected orbit rms is increased. In this case, higher values of $\Delta E/E$ can be used to reduce the error contribution from monitors.

## 9.3 Shimming of undulator field

The effect of undulator field errors can be efficiently suppressed in the simulations by choosing a short length for correcting both field integrals (see section 4). Beam alignment results are shown in fig. 16 as functions of the "shimming length" for horizontal and vertical field errors of 0, 1, 2 and 3 mT rms, i.e. 0, 0.2%, 0.4% and 0.6% of the dipole peak field $B_o$. Note that for a shimming length equal to one period length the random field error of both poles are corrected.

Correcting both field integrals every ten period lengths the undulator field errors of 2 mT rms increase the orbit rms by 3%. For longer integration lengths, the effect of dipole kick errors become larger than the rest of the orbit kick errors and lead to large orbit distortions. If the effect on the orbit angle rms has to be taken into account for the SASE process, the shimming interval must be reduced to very few period lengths.

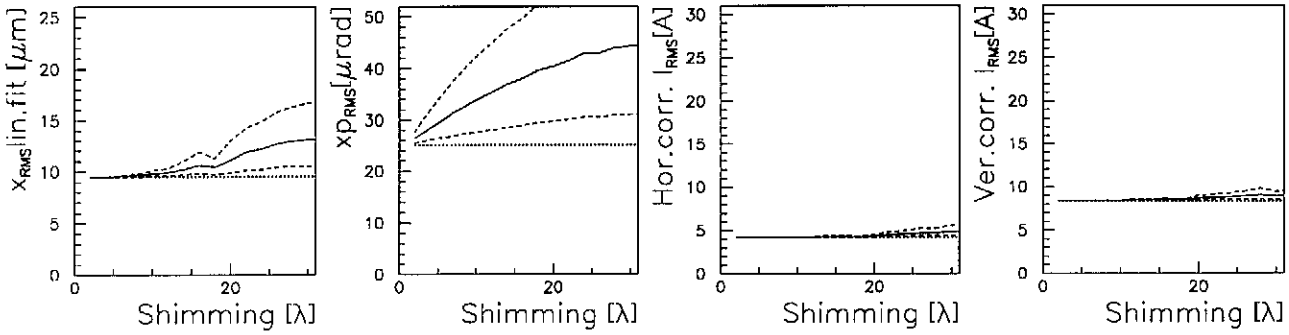


Figure 16: Mean $x_{\rm rms}$ (linear fit), $x'_{\rm rms}$ and corrector current rms as functions of the shimming length in units of period lengths. Results for $\Delta B = 2$ mT rms are indicated with a solid line. The dashed lines are the results for $\Delta B = 0$, 1, 2 and 3 mT rms.

## 9.4 Location of monitors and correctors in the FEL

The optimum location of the beam position monitors with respect to the quadrupoles of the FEL is investigated. Simulation results are shown in fig. 17 as function of the relative longitudinal position of the monitors with respect to the entrance position of the focusing quadrupole.

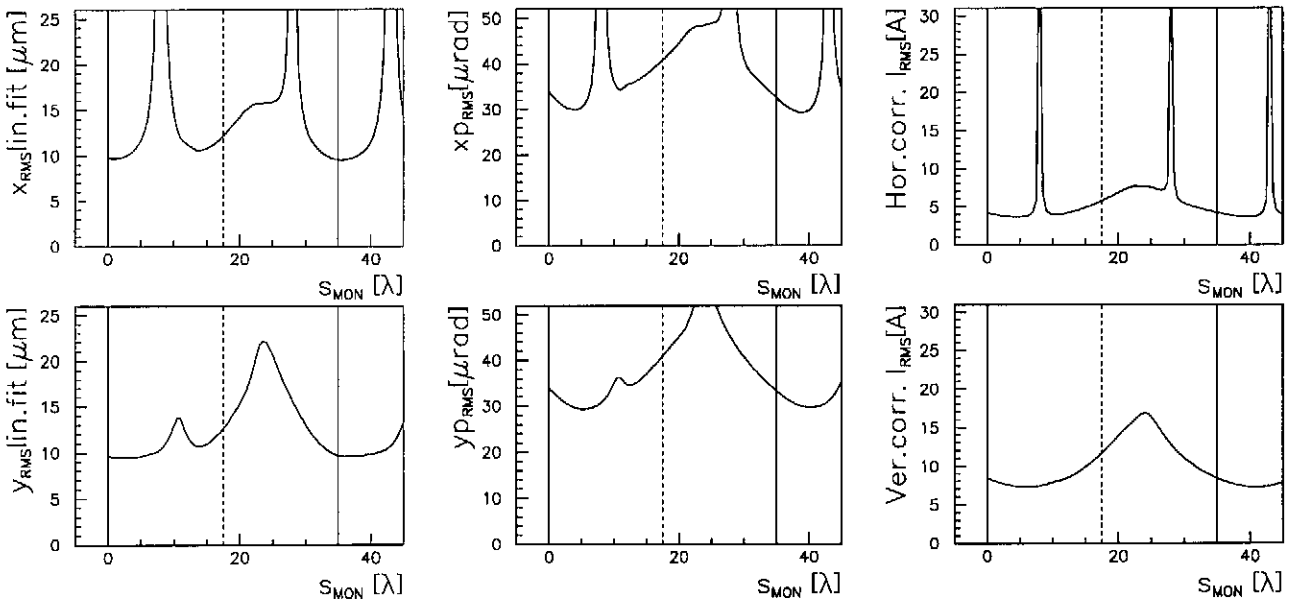


Figure 17: Mean $x_{\rm rms}$ (linear fit), $x'_{\rm rms}$ and corrector current rms for $E = 390$ MeV as functions of the distance between monitors and quadrupoles (in period length units). Vertical solid (dashed) lines indicate when monitors are placed at horizontal (de)focusing quadrupoles.

The lowest orbit rms is obtained in simulations with monitors located at horizontal focusing quadrupoles. Monitor locations between quadrupoles result in a large orbit rms. Placing the correctors at defocusing quadrupoles (indicated with vertical dotted line in fig. 17) the orbit rms is somewhat larger than at focusing quadrupoles. The reason is that the horizontal beta function is maximum at the horizontal focusing quadrupoles, therefore orbit and dispersion errors are larger at them and the effect of correctors on the orbit is enhanced. Both contributions make the dispersion correction more efficient.

Similar results are obtained at 1 GeV, which are shown in fig. 18. The ratio between the maximum and the minimum of the beta function is 1.4 which is smaller than 2.3 at 390 MeV.

Therefore the orbit rms obtained with monitors located at defocusing quadrupoles is not much larger than with monitors located at focusing quadrupoles as for 390 MeV.

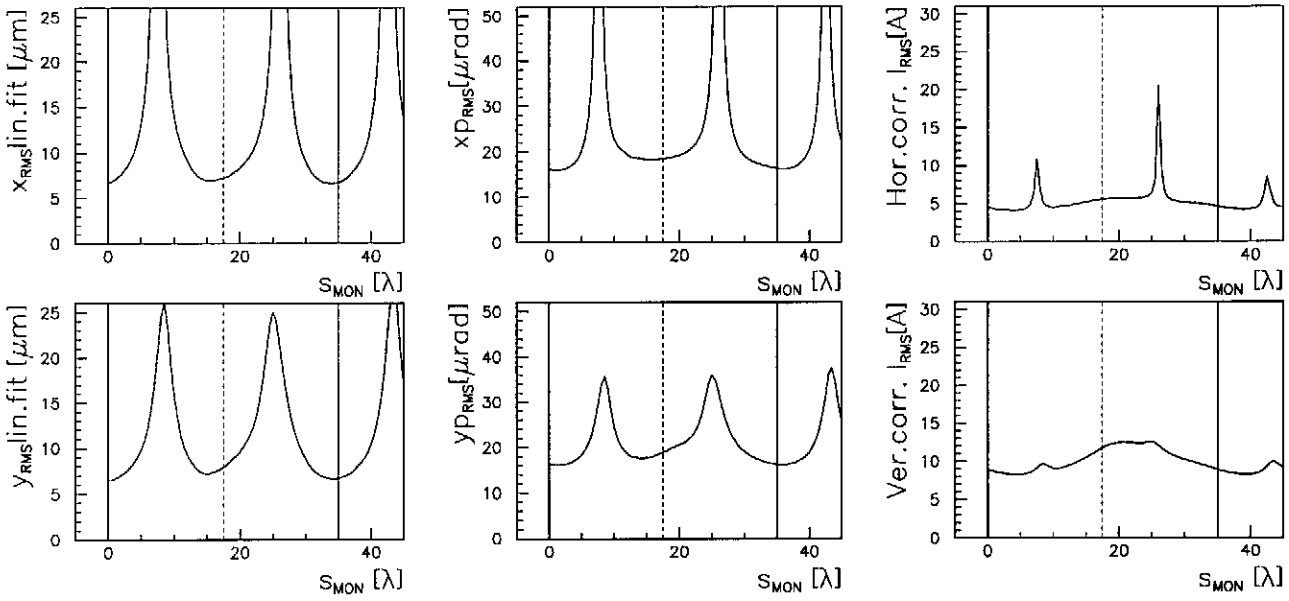


Figure 18: Mean $x_{\rm rms}$ (linear fit), $x'_{\rm rms}$ and corrector current rms for $E = 1$ GeV as functions of the distance between monitors and quadrupoles (in period length units). Vertical solid (dashed) lines indicate when monitors are placed at the entrance position of horizontal (de)focusing quadrupoles.

## 9.5 Corrector current versus length

The length of the correctors has a small effect on beam alignment results. The average integrated strength of the correctors also does not change. However, for the same integrated strength, the corrector field (and therefore its current) is inversely proportional to its length. This effect is shown in fig. 19. The maximum corrector length is limited to the distance between two monitors (about $14\lambda_u$). With the design length value $11\lambda_u$ (30 cm), the corrector occupies almost all the space available between monitors. This minimizes the current demand and therefore reduces the cost of the power supplies and the cooling system of the wires.

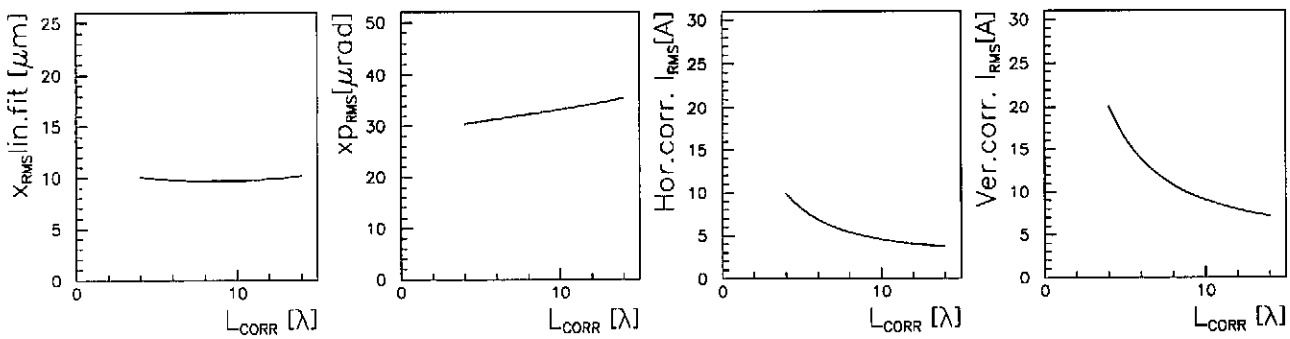


Figure 19: Mean $x_{\rm rms}$ (linear fit), $x'_{\rm rms}$ and corrector current rms as function of corrector length (in period length units) keeping the entrance position of the corrector fixed.

## 9.6 Beam orbit errors at the entrance of the undulator

Until now beam orbit errors at the entrance of the undulator are neglected. A perfect beam alignment with respect to the center of the undulator (defined as the magnetic center of the quadrupoles) is assumed and the dispersion function is taken as zero. In the case of a beam position offset or angle at the entrance of the undulator the orbit is brought towards the center of the undulator using the dispersion correction scheme. An example of such an orbit correction is shown in fig. 20 in a simulation for a perfect quadrupole alignment, a field error free undulator and no monitor errors.

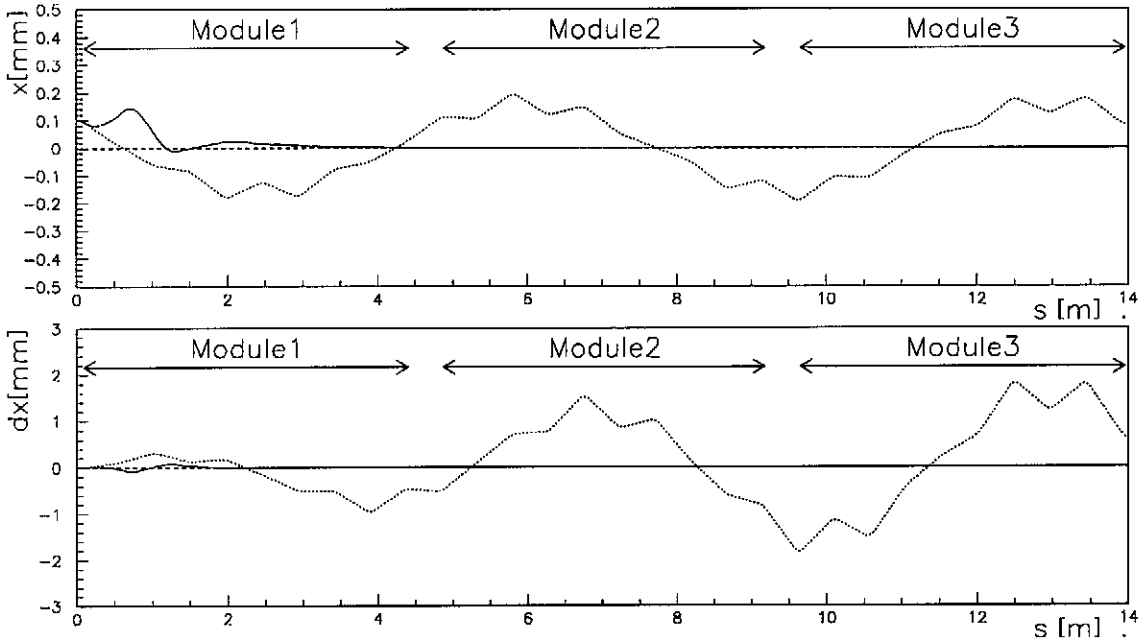


Figure 20: Horizontal orbit with an initial offset of 0.1 mm (top plot) and dispersion $d_x$ (bottom plot) before (dotted line) and after correction (full line).

The orbit distortion due to beam misalignment at the entrance of the FEL is corrected within the first module. The dispersion created by this misalignment is minimized to a small dispersion bump at the first module of the FEL. The beam is then aligned with respect to the center of the undulator.

An example of the correction of an incoming dispersion offset is shown in fig. 21 in a simulation including no other errors. Dispersion errors at the entrance of the FEL do not affect the beam orbit in the FEL and does not change the orbit rms. However, it affects the result of dispersion corrections applied to the FEL. The initial dispersion is corrected in the first module by displacing the orbit from the center ($x = 0$) and creating a "closed bump".

A dispersive beam at the entrance of the FEL is corrected while introducing a displacement of the orbit. Both orbit and dispersion are vanishing at the second module.

## 9.7 Alignment of FEL modules

A perfect alignment of the FEL modules is assumed in the previous simulations. Errors on the position and the angle of the modules changes the relative position of the quadrupoles with respect to the incoming beam.

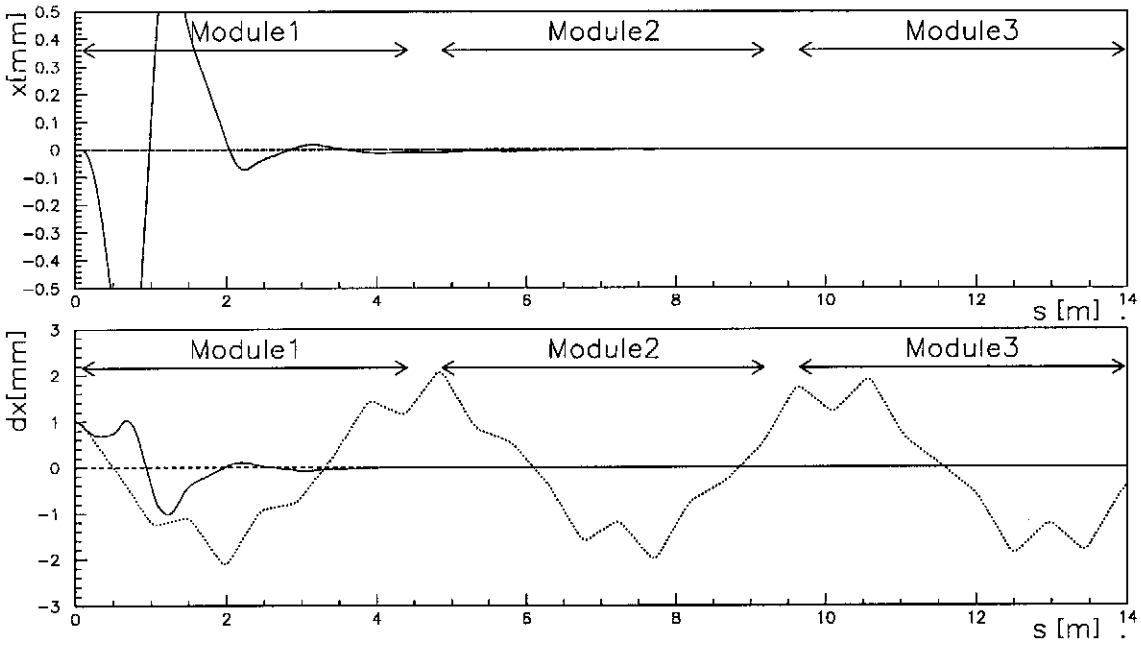


Figure 21: Orbit $x$ (top plot) and dispersion $d_x$ with an initial offset of 1 mm (bottom plot) before (dotted line) and after correction (full line).

In each module, a random position error with a flat distribution between $\pm\Delta x_{\mathrm{mod}}$ is added to the individual random position error of the quadrupoles. Results are shown in fig. 22 as functions of the random error amplitude $\Delta x_{\mathrm{mod}}$. An increase of about 25% on the corrected orbit rms is observed for module position errors between $\pm 30$ $\mu$m.

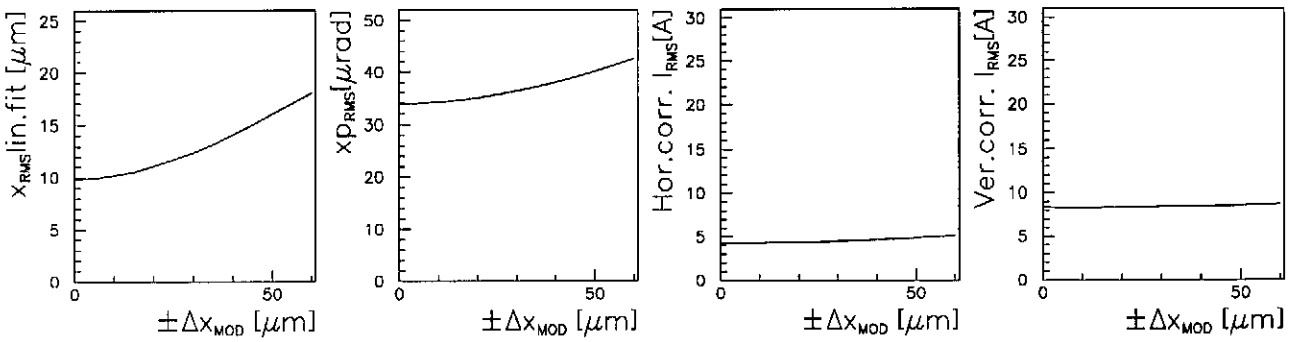


Figure 22: Mean $x_{\mathrm{rms}}$ (linear fit), $x'_{\mathrm{rms}}$ and corrector current rms as functions of the position error of the FEL modules.

# 10 Conclusions

Beam-based alignment by dispersion correction was simulated for the TTF-FEL. Simulations included quadrupole misalignment errors between $\pm 50$ $\mu$m, horizontal and vertical dipole field errors of 2 mT (0.4% of peak field) rms and monitor measurement errors of 1 $\mu$m rms. An orbit rms of about 10 $\mu$m is in average obtained for a beam energy of 390 MeV. This result is obtained with one monitor every quadrupole and with one horizontal corrector per horizontal focusing quadrupole and one vertical corrector per vertical focusing quadrupole. The current rms for horizontal correctors is 4.2 A and for vertical correctors is 8.3 A. In simulations using only the

monitors at focusing quadrupoles, the orbit rms increases up to 3%. An increment of about 15% for the orbit rms and of 3% for the corrector current rms are found if only the monitors at defocusing quadrupoles are used. The monitors of the last two quadrupoles and one monitor at the end of the undulator allow a global dispersion correction, which efficiently reduces the orbit rms.

The effect of dipole field errors on the orbit is minimized by correcting the first and the second field integrals over ten period lengths (in both horizontal and vertical planes). The effect of monitor measurement errors on the corrected orbit is minimized by choosing a large $\Delta E/E$ for dispersion measurements. For 1 $\mu$m rms monitor resolution, the dispersion is calculated from the difference orbit of a beam with $E$ and $E - \Delta E$, with $\Delta E/E$ =0.2.

Beam misalignment and dispersion errors at the entrance of the undulator affect the result of beam-based alignment in the first part of the undulator. The dispersion correction scheme can correct these orbit errors. Therefore, it is desirable to apply this scheme to the FEL including the beam line previous to the undulator.

# References


[1] *A VUV Free Electron Laser at the TESLA Test Facility at DESY, Conceptual Design Report*; DESY/TESLA-FEL 95-03, June 1995.

[2] R. Bonifacio, C. Pellegrini and I.M. Narducci; *Collective Instabilities and High-Gain Regime in a Free Electron Laser*; Opt. Commun. 50 (1984) 373.

[3] B. Faatz, J. Pflüger and Y.M. Nikitina; *Study of the Undulator Specification for the VUV-FEL at the TESLA Test Facility*; DESY/TESLA-FEL 96-13 and Proc. of the 1996 FEL Conf., Rome, August 1996.

[4] M. Böge and R. Brinkmann; *Optimization of Electron Spin Polarization by Application of a Beam-Based Alignment Technique in the HERA Electron Ring*; Proc. of the 4th Inter. Workshop on Accel. Alignment, Tsukuba, November 1995.

[5] B. Autin and Y. Marti; *Closed Orbit Correction of A.G. Machines using a Small Number of Magnets*; CERN/ISR-MA/73-17, March 1973.

[6] J. Pflüger, Y.M. Nikitina, B. Faatz and T. Teichmann; *The undulator system for the VUV-FEL at the TESLA Test Facility*; DESY/TESLA-FEL 96-13 and Proc. of the 1996 FEL Conf., Rome, August 1996.

[7] W. Brefeld, B. Faatz, Yu.M. Nikitina, J. Pflüger, P. Pierini, J. Roßbach, E.L. Saldin, E.A. Schneidmiller, M.V. Yurkov; *Parameter study of the VUV FEL at the TESLA Test Facility*; Nucl. Instr. Meth. A375 (1996) 295-298.

[8] J. Roßbach, priv. communication.